Accepted in Journal of the Brazilian Society of Mechanical Sciences and Engineering (BMSE) on 24.3.22

A hybrid Grey-TOPSIS based quantum behaved particle swarm optimization for selection of electrode material to machine Ti6Al4V by electro-discharge machining

Anshuman Kumar Sahu[1*], Siba Sankar Mahapatra[1], Marco Leite[2] and Saurav Goel[3,4]
[1]Department of Mechanical Engineering, National Institute of Technology Rourkela, Rourkela-769008, Odisha, India
[2]IDMEC, Instituto Superior Técnico, Universidade de Lisboa, Lisboa, Portugal
[3]School of Engineering, London South Bank University, 103 Borough Road, London SE1 0AA, UK
[4] University of Petroleum and Energy Studies, Dehradun, 248007, India

[*] E-mail: anshuman.sahu123@gmail.com

Abstract: Electro-discharge machining is an extensively used manufacturing process. The process requires a tool electrode but the selection of the right material for preparing the tool continues to remain an engineering puzzle. This work makes use of a hybrid intelligent algorithm for selecting the right electrode out of three tool electrodes such as AlSi10Mg, copper and graphite for efficient electro-discharge machining of Ti6Al4V. The work began by constructing a Taguchi's L_{27} experimental design and then collecting the output data such as the material removal rate, tool wear rate, surface roughness, surface crack density, white layer thickness and micro-hardness. A simultaneous multi-objective optimization was performed to maximise the workpiece material removal rate while minimizing the remaining variables. For this purpose, a hybrid grey-TOPSIS based quantum-behaved particle swarm optimization was chosen and additional data gathered from scanning electron microscopy and energy dispersive spectroscopy techniques revealed new insights into the post-machining material behaviour such as the use of graphite electrode makes the machined surface far harder due to the dissociated carbon.

Keywords: additive manufacturing (AM); electro-discharge machining (EDM); tool electrode; grey-TOPSIS; optimization; quantum behaved particle swarm optimization (QPSO)

1. Background and motivation

Electro-discharge machining (EDM) is a commonly used non-traditional machining process in which material removal occurs by recurring electrical sparks between two electrodes (tool electrode and work electrode) separated by a dielectric fluid. EDM is usually preferred to cut difficult-to-cut (usually conductive) materials such as tool steel, nickel based alloys, titanium based alloys and metal matrix composites in molds and dies, aerospace, automobile and biomedical sectors [1, 2]. In a typical EDM operation, the electrode and workpiece are submerged inside a dielectric fluid and the spark created by the applied voltage removes the material from the electrode and workpiece surfaces. The process alters the surface properties of the workpiece surfaces with formation of material defects such as cavities, voids, white layer, micro cracks etc. These defects adversely affect the quality of the machined surface finish of the components which eventually may dictate the lifetime, especially the fatigue life of machined parts. The problem can partly be solved by proper flushing of debris. However, flushing is not always feasible due to part complexity and difficult tool path [1, 3].

A more important decision in successful EDM of a component is associated with the right selection of the tool electrode material and its fabrication route. To save on the costs, an additive manufacturing (AM) method such as selective laser sintering (SLS) can be used to fabricate the tool electrode. By using the SLS process, one can produce a complex shaped electrode in a cost-effective and timely manner. SLS is a powder based technique in which parts are sintered in layers using a laser beam [4, 5]. However, not all materials are amenable to SLS which makes it a bit difficult to adopt any material to be fabricated by SLS. Titanium alloy (Ti6Al4V), is extensively used in aerospace such as turbine blades, airframes, aircraft engine and structural parts; in biomedical applications such as medical instruments, orthopedic implants and prosthetic valves; in defence such as missile fuel tank, jet engine [6, 7]. However, Ti6Al4V is a difficult-to-cut material by a single point cutting tool and therefore, EDM can be more economical to machine complex shapes in Ti6Al4V.

In an EDM process, multiple performance measures are required to be simultaneously optimized, for instance, maximization of material removal rate (MRR) and concurrent minimization of tool wear rate (TWR), average surface roughness (R_a), surface crack density (SCD), white layer thickness (WLT) and micro-hardness (MH) of the machined surface. In this work, a hybrid optimization technique like Grey-TOPSIS based QPSO is used for concurrent optimization of all the performance output measures. This area of research especially the preparation of tool electrodes by the SLS process is still infancy stage and hence this simultaneous optimization of the performance attributes concerning the tool electrode material selection became the primary motivation of this work. The novelty in this investigation lies in the selection of the optimization algorithm and the verification of the output by using the scanning electron microscope and energy dispersive X-ray spectroscopy to examine the migration mechanism of the atomic species.

2. State of the art

The literature of past work reveals that machining of titanium alloys using electro-discharge machining process [1, 8-14] is quite a popular topic of investigation. However, very few works have been done on the EDM of Titanium alloys using tool electrodes fabrication by the SLS process. Among others, Sahu and Mahapatra [15] studied the performance of the SLS electrode during EDM of titanium alloy. They considered performance measures such as MRR, TWR and R_a and observed a superior finish of the components while using the SLS electrode in comparison to the use of copper and graphite electrodes. However, the post machining workpiece surface integrity and surface morphology were not adequately examined by them. Uhlmann et al. [3] manufactured a WC-Co electrode by selective laser melting (SLM) process and compared its performance with copper, graphite and tungsten carbide electrodes during EDM of tool steel. The WC-Co electrode allowed higher material removal (MRR) than only WC, but lower MRR than copper and graphite electrodes, although the wear of WC-Co electrode compared to the other electrodes was highest. Different composition of electrodes such as ZrB_2-CuNi, TiB_2-CuNi, Mo-CuNi were prepared by the SLS process and used successfully in the EDM process [5, 16-18]. Amorim et al.[19] manufactured pure copper, bronze–nickel, copper-bronze–nickel and steel electrodes by the SLS process and studied their performance for EDM of tool-steel workpiece. The performance of these electrodes was examined under three machining conditions such as finish, semi-finish and roughing operations by considering MRR and tool wear. It was found that the performance of these electrodes

was inferior to the solid copper electrodes. Durr et al.[20] prepared the bronze-nickel-copper electrode by the SLS method and studied their performance to machine the X210Cr12 steel and C45 steel. They found that an increase in porosity in electrode increases the electrode wear and that the electrode wear for machining X210Cr12 steel was more than C45 steel.

Meena and Nagahanumaiah[21] manufactured the Cu-Ni-Sn-P electrode by direct metal laser sintering (DMLS) method and analyzed its performance during the machining of EN-24 steel. They found the current was the most significant parameter that influence MRR, TWR and Ra as compared to pulse-on-time and flushing pressure. Zhao et al.[22] manufactured the SLS electrode from steel, phosphate and polyester as a binder and its performance was studied during EDM of 45 steel workpieces. The TWR was observed to increase with an increase in pores and holes in the electrode. Tang et al.[23] manufactured Cu-W, Cu-W-Ni, Cu-B4C and Cu-B4C-Ni electrodes by laser cladding process and studied their performance during the EDM of mild steel workpiece. These electrodes showed a lower removal rate and wear rate as compared to commercially available pure copper electrodes. Tay and Haider[24] manufactured bronze-nickel electrode by the DMLS process and performed electroless copper deposition on it to improve surface finish and conductivity. The performance of the DMLS electrode was studied by taking hardened tool steel as workpiece material for rough cutting, semi-rough cutting, finish cutting. In the case of the DMLS electrode, TWR was high and MRR was low for both roughing and semi roughing and was found suitable for applications where minimum MRR is required.

This brief review of the literature shows contradictory explanations concerning different types of traditional electrodes and the electrode manufactured by the SLS method. This research work makes use of AlSi10Mg powder for preparing the EDM electrodes owing to its good electrical conductivity and good wear resistance during sparking and ease of processing by the SLS process. Here, the performance of AlSi10Mg SLS electrode was studied and benchmarked to the conventionally used copper and graphite electrodes (prepared by the mechanical turning) to machine Ti6Al4V using the EDM process.

3. Materials and methods

3.1 Workpiece and tool electrode material

To manufacture a complex-shaped electrode, the selective laser sintering (SLS) method can be used. In this work, AlSi10Mg powder was used to fabricate the electrode by the SLS process. The SLS machine used for the manufacturing of the electrode was EOSINT M 280 (EOS, Germany). The electrode manufactured is cylindrical with varying diameter having a machining diameter of 25 mm. Similarly, copper and graphite electrodes were fabricated by taking a solid cylindrical rod by the conventional turning process with a machining diameter of 25 mm. The three electrodes used for the EDM process are shown in Fig. 1. The workpiece of Ti6Al4V used had dimensions 60×60×10 mm and commercial grade Rustlick EDM-30 oil was used as the dielectric medium.

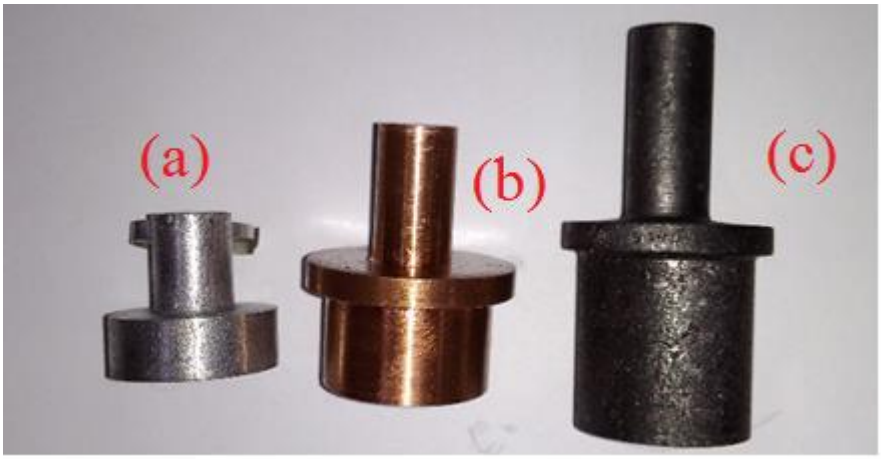

Fig. 1. Tool electrodes (a) AlSi10Mg, (b) Copper and (c) Graphite[15]

3.2 Experimental procedure and data collection

To investigate the performance of the EDM process, a die-sinking EDM (model: ELECTRA EMS-5535, Electronica, India) was used. Here, straight polarity (where a workpiece as anode and electrode as cathode) was used. During machining, the process parameters such as the voltage (V), peak current (I_p), duty cycle (τ), pulse duration (T_{on}) and tool type were varied following a design of experimental scheme proposed by Taguchi[25] (see Table 1 and Table 2). Here a five-factor-three-levels were used for preparing the Taguchi's L_{27} design of experiment (DOE) array to perform every EDM experiment for 10 minutes.

The MRR and TWR were estimated using the weight loss criteria of the workpiece and electrode during machining. The weight of the workpiece and electrodes were measured before and after each experimental run by precision balance (with a least count of 0.001g) using Eq. (1) and (2) respectively.

$$MRR = \frac{\Delta W_p}{T \times \rho_w} \tag{1}$$

$$TWR = \frac{\Delta W_e}{T \times \rho_e} \tag{2}$$

where, ΔW_p is the weight loss from workpiece during machining, ΔW_e is the weight loss from electrode during machining, T is the machining time (10 min), ρ_w is the density of workpiece (4.42 g/cm^3) and ρ_e is the density of electrodes (for AlSi10Mg ρ_e=2.664 g/cm^3, for copper ρ_e=8.96 g/cm^3 and for graphite ρ_e=2.267 g/cm^3).

A Taylor-Hobson (PNEUNO-Suetronic 3+) was used to take three roughness measurements in the transverse direction. The average of these three readings was recorded as the average surface roughness (R_a). The SCD and WLT were measured by taking the micro-images of the machined surface using a scanning electron microscope (SEM) (model: Jeol JSM-6480LV, Japan). SEM images of the machined surfaces were taken at three locations and corresponding surface cracks were measured by PDF-XChange viewer software. The total surface crack length divided by the micro-image area was considered as the SCD and the average of these three was recorded for the optimization purposes. Similarly, for WLT, the machined surface was cut into sizes of 10×10×10 mm^3 by a wire-EDM and the

transverse section of the machined surface was polished and etched with Kroll's etchant. The corresponding SEM images were used to estimate the WLT using the ImageJ software.

Vicker's micro-hardness tester (LECO LM248AT, USA) was used to measure the MH on the white layer over the machined surface with a testing load of 50gf and micro-indentation dwell time of 10s. MH at three positions on the middle position of the white layer was taken and the average of these three was considered for the analysis. The final measurement values for the SCD and WLT are shown in Fig. 2. The outputs of the experiments are shown in Table 2. The parallel coordinated graph for all the performance measures in normalized form is shown in Fig. 3. In Fig. 3, the minimum and maximum values for each category are presented in the X axis and in Y axis the normalized performance measures are presented. It showed the conflicting nature of all the performance measures in EDM process, that need to optimize to get best parametric setting by considering all the performance measures simultaneously.

Table 1. Factors and levels used in the experimental study

Parameters	Unit	Level 1	Level 2	Level 3
A-Voltage (V)	V	20	25	30
B-Peak current (I_p)	A	10	15	20
C-Duty cycle (τ)	%	67	75	83
D-Pulse duration (T_{on})	µs	100	200	300
E- Electrode type	-	AlSi10Mg SLS (1)	Copper (2)	Graphite (3)

Table 2. Experimental design and performance measures

S.N .	A	B	C	D	E	MRR (mm^3/min)	TWR (mm^3/min)	R_a (µm)	SCD (µm/$µm^2$)	WLT (µm)	MH ($HV_{0.05}$)
1	20	10	67	100	1	0.5454	0.6706	6.4	0.0145963	17.0278	509.0
2	20	10	67	100	2	0.5820	0.6898	6.7	0.0157017	20.2074	581.5
3	20	10	67	100	3	1.0643	0.4955	8.2	0.0204210	21.7504	616.5
4	20	15	75	200	1	0.9226	1.5553	7.2	0.0145963	22.2146	616.9
5	20	15	75	200	2	0.9654	1.0678	7	0.0204913	34.0527	731.5
6	20	15	75	200	3	1.3029	0.5744	8.3	0.0214737	27.6974	816.5
7	20	20	83	300	1	1.4221	1.5100	7.8	0.0246667	24.2642	965.7
8	20	20	83	300	2	1.4516	1.5529	8.3	0.0275790	44.4150	1098.2
9	20	20	83	300	3	1.6093	0.8402	9.2	0.0309123	45.8311	1124.5
10	25	10	75	300	1	0.8291	1.6003	7.2	0.0187720	31.0627	671.3
11	25	10	75	300	2	1.1820	1.3972	7.3	0.0248070	35.6386	790.2
12	25	10	75	300	3	1.1784	0.5556	8.2	0.0279297	33.1680	886.5
13	25	15	83	100	1	1.1204	1.7030	7.1	0.0188767	18.6306	765.7
14	25	15	83	100	2	1.2286	1.6353	7.4	0.0200000	26.4284	828.0
15	25	15	83	100	3	1.2890	0.5739	9.4	0.0220527	31.3732	869.6
16	25	20	67	200	1	1.3368	1.5642	7.3	0.0185613	27.4284	899.8
17	25	20	67	200	2	1.6033	1.5320	8.4	0.0244913	27.7912	1082.2
18	25	20	67	200	3	1.6753	0.2556	9	0.0290350	40.5845	1253.0
19	30	10	83	200	1	1.0109	1.6835	7.2	0.0165263	33.2624	856.7
20	30	10	83	200	2	1.2899	1.4414	7.4	0.0220350	31.8733	951.0

21	30	10	83	200	3	1.1223	0.5614	9.5	0.0237193	34.2199	1085.5
22	30	15	67	300	1	1.1701	1.5359	7.4	0.0207017	28.1340	991.7
23	30	15	67	300	2	1.3438	1.7646	7.8	0.0237893	36.7299	1106.8
24	30	15	67	300	3	1.6224	0.3751	9.6	0.0268773	39.2965	1247.4
25	30	20	75	100	1	1.3436	1.7590	8.1	0.0218420	26.5360	1020.7
26	30	20	75	100	2	1.6286	1.5441	8.4	0.0245087	34.5741	1264.7
27	30	20	75	100	3	1.7113	0.7015	9.8	0.0279297	34.3433	1670.2

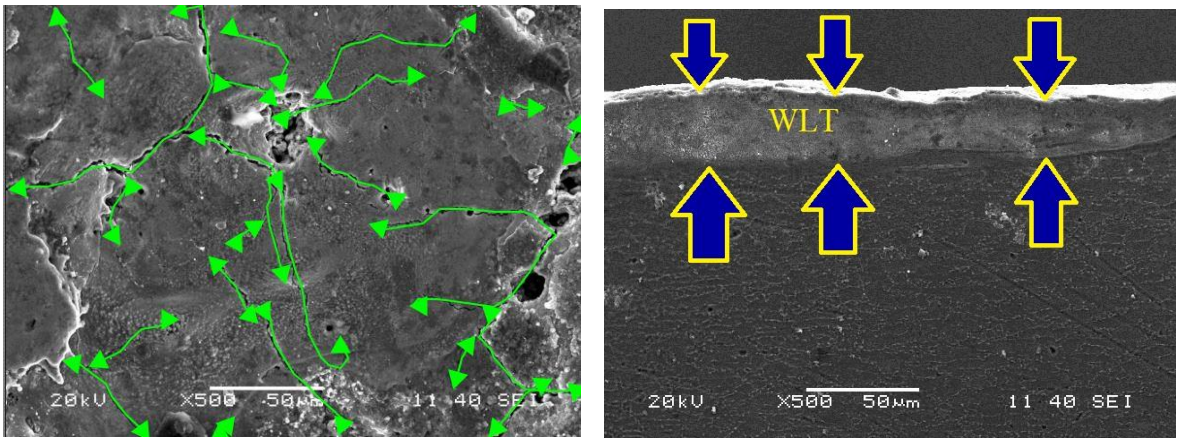

(a) SCD (b) WLT

Fig. 2. Measurement of SCD and WLT

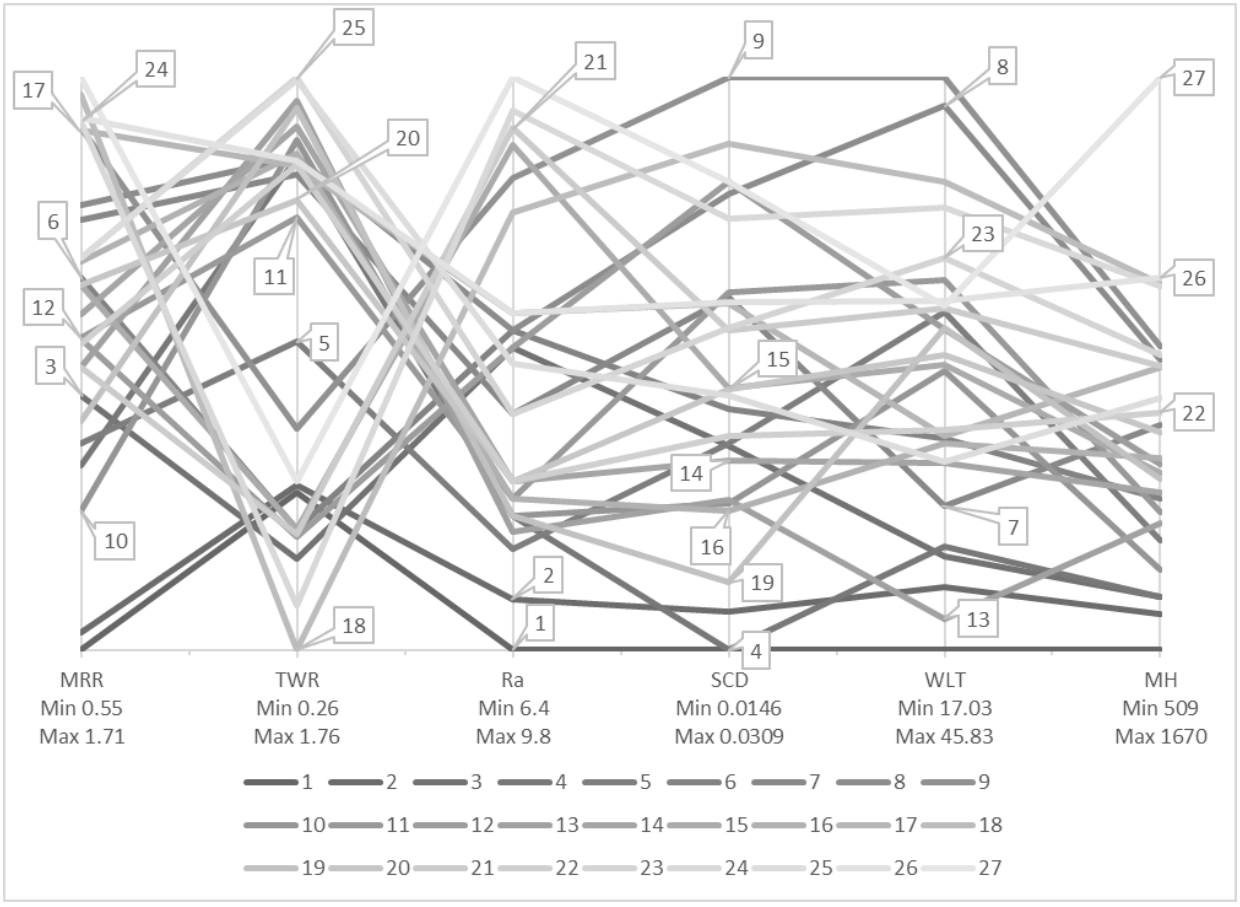

Fig. 3. Parallel coordinated graph for the performance measures

3.3 Grey-Technique for Order of Preference by Similarity to Ideal Solution (Grey-TOPSIS)

Grey-TOPSIS is a multi-objective hybrid optimisation approach used in this work for concurrent optimization of the various objective functions desired in this work. Deng[26] developed a grey relational analysis (GRA) technique from the grey system theory. GRA is a multi-objective optimisation approach that delivers an efficient solution of multi-objective problems. In this technique, the data is processed in the initial step to neutralize all the performance measures of the different units to a range of 0 to 1. Then grey relational coefficients are generated from the normalized output data followed by the generation of grey relational grade. The substitute having the highest value of grey relational grade is chosen as the best substitute[2, 27]. Similarly, TOPSIS is also used as a multi-response optimisation technique for the selection of optimal parameters to maximise the preferred performances and simultaneously minimize the un-preferred performances to increase the efficiency. Here, two artificial alternative solutions are considered such as the best and worst solutions. It concurrently measures the distance of the alternatives from the best (positive ideal) solution and worst (negative ideal) solution. The alternatives are selected from the nearest positive ideal solution and from the farthest negative ideal solution. Then a relative closeness from the ideal solution is calculated and the alternative having the highest relative closeness value is considered as the best alternative[28].

Grey-TOPSIS is a hybrid optimisation method that encompasses the beneficial characteristics of both GRA and TOPSIS methods and is widely used in supply chain and assignment tasks[29-31]. However, the Grey-TOPSIS approach has been rarely utilised for optimisation in manufacturing work. The procedure of the hybrid Grey-TOPSIS method is described below.

1. Calculate the normalized value (Y_{ij}) of performance output measures.

For smaller-is-better, $$Y_{ij} = \frac{y_{ij}^{max} - y_{ij}}{y_j^{max} - y_j^{min}} \quad (3)$$

For higher-is-better, $$Y_{ij} = \frac{y_{ij} - y_{ij}^{min}}{y_j^{max} - y_j^{min}} \quad (4)$$

where y_{ij} = obtained data for i^{th} experiment in j^{th} response.

y_j^{max} = highest value of the j^{th} response.

y_j^{min} = lowest value of the j^{th} response.

2. Calculate the grey relational coefficient (γ_{ij}).

$$\gamma_{ij} = \frac{(\Delta_j^{min} + \xi\Delta_j^{max})}{(\Delta_{ij} + \xi\Delta_j^{max})} \quad (5)$$

where $\Delta_{ij} = |1 - Y_{ij}|$

$\Delta_j^{min} = \min(\Delta_{1j}, \Delta_{2j}, \ldots\ldots\ldots \Delta_{mj})$ $\quad \Delta_j^{max} = \max(\Delta_{1j}, \Delta_{2j}, \ldots\ldots\ldots \Delta_{mj})$

where Δ_{ij} = deviation sequence, ξ = distinguishing coefficient, $\xi \in [0,1], \xi = 0.5$

3. Form the decision matrix with ‘m’ number of attributes and ‘n’ numbers of alternatives as presented in Eqn. (6).

$$D_m = \begin{bmatrix} \gamma_{11} & \gamma_{12} & \gamma_{13} & L & L & \gamma_{1m} \\ \gamma_{21} & \gamma_{22} & \gamma_{23} & L & L & \gamma_{2m} \\ \gamma_{31} & \gamma_{32} & \gamma_{33} & L & L & \gamma_{3m} \\ M & M & M & O & O & M \\ M & M & M & O & O & M \\ \gamma_{n1} & \gamma_{n2} & \gamma_{n3} & L & L & \gamma_{nm} \end{bmatrix} \quad (6)$$

4. Form weighted normalized matrix (v_{ij}) by multiplying the weighted value with the decision matrix.

$$v_{ij} = w_j \times \gamma_{ij} \quad (7)$$

Where, $i = 1, 2, ...n$, $j = 1, 2.....m$ and $\sum w_j = 1$

5. Calculate the ideal experimental run that are the best (S^+) and the worst (S^-) experimental run performance for each experiment.

$$S^+ = \left[\max(v_{ij}) \middle| j \in J\right] \text{or} \left[\min(v_{ij}) \middle| j \in J'\right], i = 1, 2, ...n, \quad (8)$$

$$S^- = \left[\min(v_{ij}) \middle| j \in J\right] \text{or} \left[\max(v_{ij}) \middle| j \in J'\right], i = 1, 2, ...n \quad (9)$$

Where, J is best attributes set of and J' is worst attributes set.

6. The performance of the performance output responses were calculated by the best experimental run distance (D_{ij}^+) from the S^+ values and the worst experimental run distance (D_{ij}^-) from the S^- values as follows.

$$D_{ij}^+ = \sqrt{\sum_{i=1}^{m} (v_{ij} - S_j^+)^2}, \quad (10)$$

$$D_{ij}^- = \sqrt{\sum_{i=1}^{m} (v_{ij} - S_j^-)^2}, \text{ where, } i = 1, 2, ...n \quad (11)$$

7. Calculate closeness coefficient (C_i) for each set of experiment by using the equation as follows.

$$C_i = \frac{D_i^-}{D_i^- + D_i^+}, i = 1, 2, ...n; 0 \le C_i \le 1. \quad (12)$$

The best optimum parameters were selected based on high value of closeness coefficient that was close to the ideal solution.

3.4 Quantum behaved particle swarm optimisation (QPSO)

Particle swarm optimisation (PSO) is an evolutionary computational technique influenced from the behaviour of bird flocking. In PSO, the population of the prospective solutions is termed a swarm and every individual solution inside the swarm is termed a particle[32]. All particles move around a search space with a velocity that is continuously revised by the individual involvement of particle and particle's neighbour's contribution or whole swarm's contribution. The swarms of the population are

maintained through the process of searching to share the exchange of information between all individuals to direct the search in the direction of the best position within the search space. Every particle travels to its best previous position and to the best particle in the entire swarm, termed as 'g_{best}', based on the global neighbourhood. Every particle travels to its best previous position and to the best particle in its restricted neighbourhood depending upon the local variant termed as 'p_{best}' model. All the particles try to converge to the base solution quickly even in the local space. All the particles try to converge towards the best solution quickly and each particle has a fitness value and the optimisation process involves finding the minimum fitness value for every particle[32, 33].

The main weakness of PSO is that it does not assurance global convergence due to the trap of it in the local optima although it does converge fast. This is because the velocity vector adopts very small values as the iterations continue. Therefore, PSO has a chance to trap in the local minima and lose its exploration and exploitation ability. To overcome this drawback of PSO, along with the concept of global convergence, an improved PSO termed as quantum behaved particle swarm optimization (QPSO) has been developed[34, 35]. In QPSO, a particle is defined by a wave function $\psi(X,t)$ in place of position (X_i) and velocity (V_i) like the PSO. The difference between PSO and QPSO is the dynamic behaviour of the swarm i.e. the exact value of position (X_i) and velocity (V_i) cannot be determined concurrently in QPSO. In QPSO, the probability of the swarm's looking in position (X_i) is learned from the probability density function $|\psi(X,t)|^2$. The probability density function is used to estimate the probability distribution function of the swarm's position. The swarm position is updated using the equations shown below[35-37].

$$X^j_{i,(t+1)} = P^j_{i,(t+1)} - \beta \times (M_{Best^j_t} - X^j_{i,t}) \times \ln(\frac{1}{u}), \quad \text{if } k \geq 0.5 \tag{13}$$

$$X^j_{i,(t+1)} = P^j_{i,(t+1)} + \beta \times (M_{Best^j_t} - X^j_{i,t}) \times \ln(\frac{1}{u}), \quad \text{if } k < 0.5 \tag{14}$$

$$P^j_{i,(t+1)} = \theta \times P_{Best^j_{i,t}} + (1-\theta) \times g_{Best^j_t} \tag{15}$$

$$M_{Best^j_t} = \frac{1}{N} \sum_{i=1}^{N} P_{Best^j_{i,t}} \tag{16}$$

where, P_i = local attractor,

$P_{Best^j_{i,t}}$ = best position of swarm 'i' at iteration 't' in respect to j^{th} dimension

$g_{Best^j_{i,t}}$ = best position, that is termed as the mean of all the best positions of the population in present generation

k, u, θ = random numbers distributed equivalently between [0, 1]

β = tuning parameter to regulate the convergence speed of the swarm. It is called a contraction expansion coefficient (CE) and its value is tuned between 0.4 to 1. It is the only parameter in QPSO that is tuned for the control of the convergence speed of the algorithm.

$$\beta = \beta_{max} - [(\beta_{max} - \beta_{min}) \times (\frac{t_i}{t_{max}})] \tag{17}$$

where, β_{max} = initial contraction expansion coefficient value

β_{min} = final contraction expansion coefficient value

t_i = current iteration number

t_{max} = maximum number of iterations

The termination condition of the algorithm is the maximum number of iterations. The QPSO algorithm in flow chart is presented in Supplementary Fig. 1.

4 Results and discussions

4.1 Grey-TOPSIS analysis

Herein, Grey-TOPSIS was used to convert all the performance outputs into a single output performance measure called a closeness coefficient (C_i). Major attention was given to maximizing the MRR and simultaneous minimization of TWR, R_a, SCD, WLT and MH. These performance measures have the most vital influence on the cost and productivity of the EDM process. Therefore, each performance output measures were converted into a normalized value by using Eq. (3) and (4) as shown in Supplementary Table 1. Here, the higher-is-better criterion was chosen for MRR and the lower-is-better criterion was chosen for the R_a, SCD, WLT and MH. In the next step, all the normalized performance measures were being converted into grey relational co-efficient using Eq. (5) as presented in Supplementary Table 2. Then a discussion matrix (Eq. (6)) was formed by considering all the grey relational co-efficient. Afterward, a normalized value decision matrix was formed by using Eq. 7 as presented in Supplementary Table 3. To form the normalized value decision matrix, an equal weightage of 0.1667 was considered. Finally, the best experimental run distance and the worst experimental run distance were calculated by following the procedure presented in Eq. (8) to (11) as shown in Supplementary Table 4. Similarly, the closeness coefficients were calculated by using Eq. (12) which are also presented in Supplementary Table 4.

4.2 Regression equation generation and optimization by QPSO

By taking the data of closeness coefficient (C_i) from Supplementary Table 4 as the output performance measure and input as the machining parameters, a non-linear regression analysis was performed by using SYSSTAT 13 software and a non-linear regression equation was developed as shown in Eq. 18 with a coefficient of determination (R^2) value of 99.1%. This non-linear equation was used as the objective function for the QPSO algorithm to optimise all the performance measures simultaneously to get the best parametric setting of machining variables. In evolutionary algorithms, the numeric domain is suitable. Therefore, the subjective variable tool type was converted into a continuous variable by assigning a value of 1 for AlSi10Mg tool, 2 for the copper tool and 3 for the graphite tool. This procedure was adopted for the development of the regression model and application of the QPSO algorithm.

$$f(x) = 0.648 \times A^{-0.251} \times B^{-0.131} \times C^{-0.136} \times D^{-0.267} \times E^{-0.197} \quad (18)$$

The QPSO algorithm was run in the MATLAB (version: R2014a) software. The convergence curve obtained for the QPSO algorithm is shown in Fig. 4. The algorithm was considered for a population size of 20 and a maximum number of iterations of 100. It was found that the QPSO algorithm converges fast towards the best solution and at the end of the 100 iterations, it was found that the value

of the objective functions i.e. closeness coefficient was 0.6480. The optimal parametric setting and the optimum closeness coefficient value are shown in Table 3.

Table 3. Optimum parametric setting with closeness coefficient

Parameters	V (A)	I_p (B)	τ (C)	T_{on} (D)	Electrode type (E)	Fitness value
Optimum setting	20V	10A	67%	100µs	AlSi10Mg (1)	0.6480

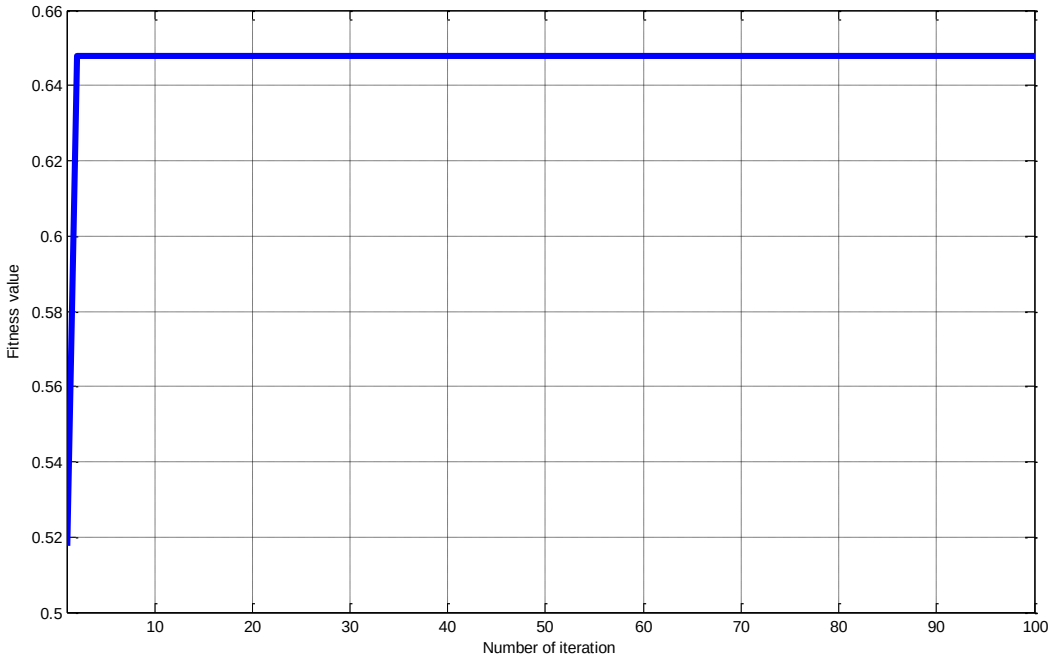

Fig. 4. Convergence curve of QPSO algorithm

4.3 Analysis of variance (ANOVA)

ANOVA a statistical test that can be used here to identify which machining parameters have significantly affected the performance measures. An ANOVA was performed for the confidence interval of 95%. The outputs from the ANOVA for the closeness coefficient are shown in Supplementary Table 5. A parameter is said to be significant if the probability of significance (P-value) is less than 0.05 ($P \leq 0.05$). It was found that all the machining parameters had a significant effect on the closeness coefficient (C_i) i.e. combine performance measure. The higher values of coefficient of determination (R^2) i.e. 95.1% describe the goodness of fit for the models at the selected confidence interval.

4.4 SEM and EDX analysis

A spark during the EDM generates very high temperatures leading to thermal stresses on the machined work surface which can cause micro-cracks. These micro-cracks become responsible for early failure of the machined components. Hence, identifying machining conditions to reduce the micro-cracks will make the EDM process more reliable. The micrographs of the machined work surface processed by the three electrodes inspected by the scanning electron microscope (SEM) are shown in Fig. 5. Fig 5 highlights the surface crack densities (SCD) on the machined work surfaces. It may be seen that AlSi10Mg SLS electrode caused less SCD followed by copper and graphite electrodes. Similarly, the

micro-graphs of the transverse section of the machined surface shows the extent of white layer thickness (WLT)) on the machined surfaces in Fig. 6.

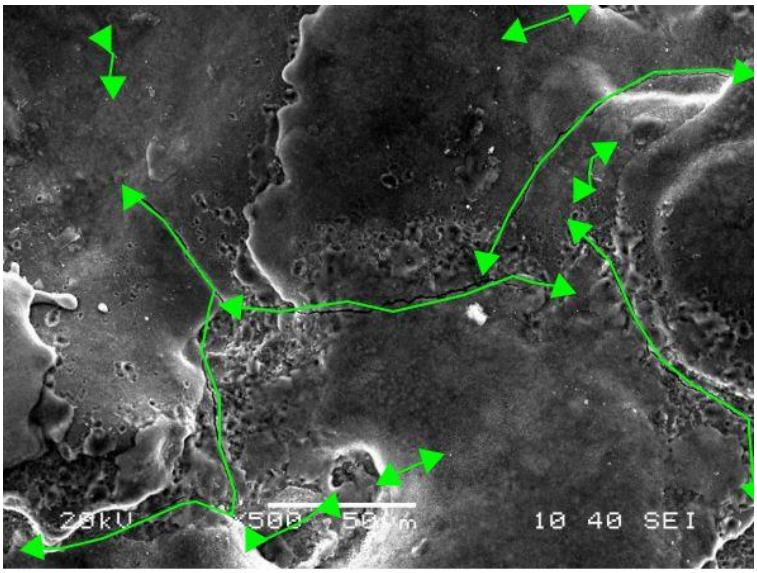

(a) SCD= 0.0145963 µm/µm^2

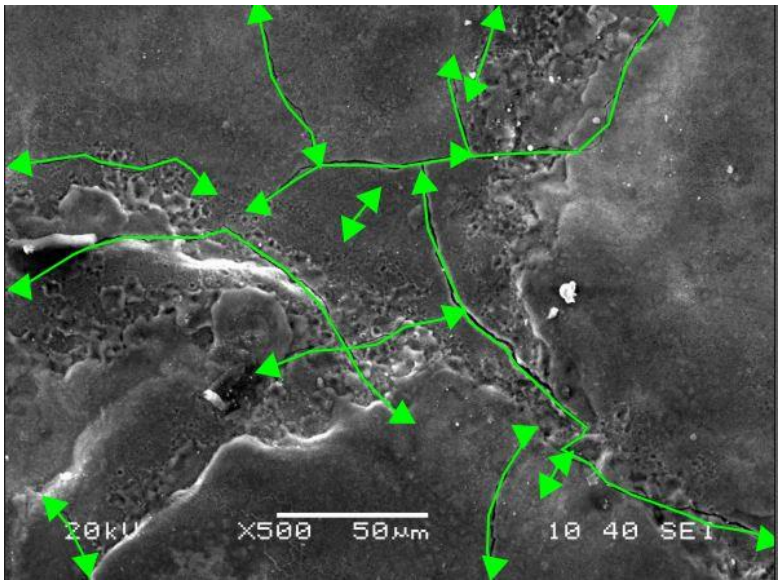

(b) SCD= 0.0157017µm/µm^2

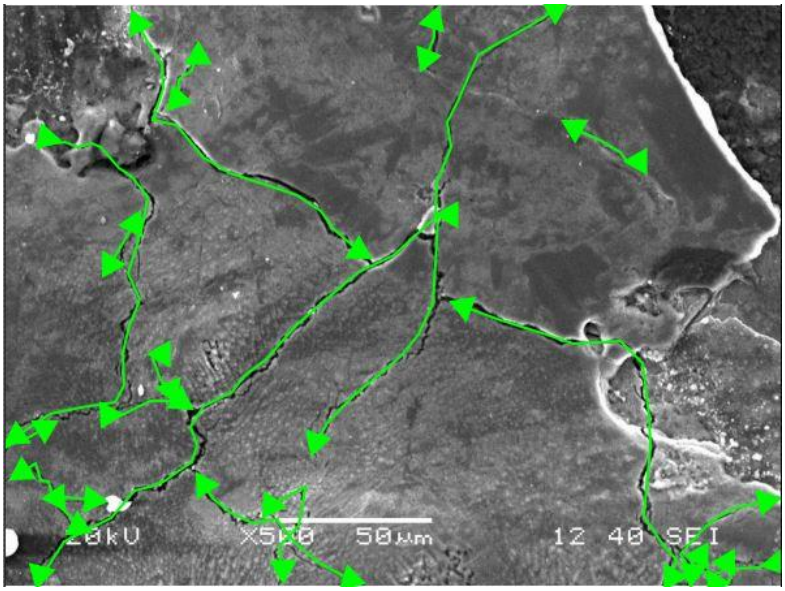

(c) SCD= 0.0204210 µm/µm^2

Fig. 5. SCD on the machined work surface by three electrodes at parameters setting V=20V, I_p=10A, τ=67%, T_{on}=100µs (a) AlSi10Mg SLS, (b) Copper, (c) Graphite

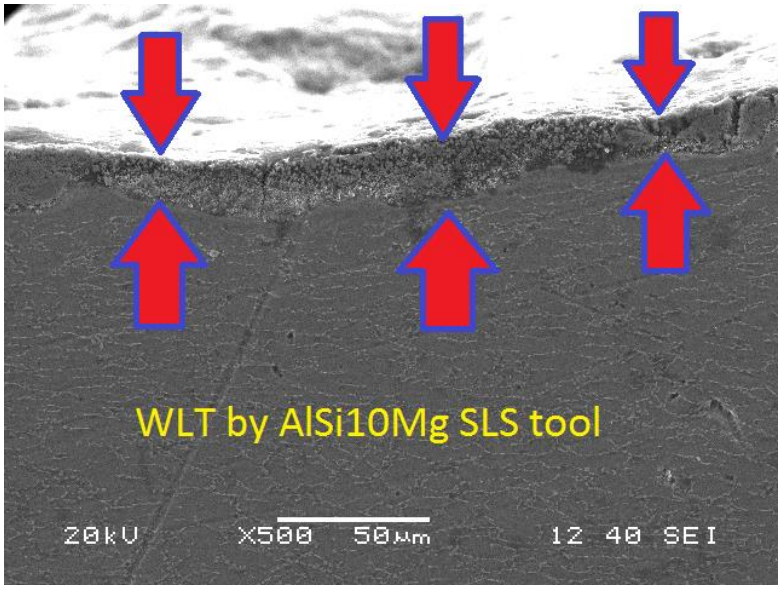

(a) WLT= 17.0278 µm

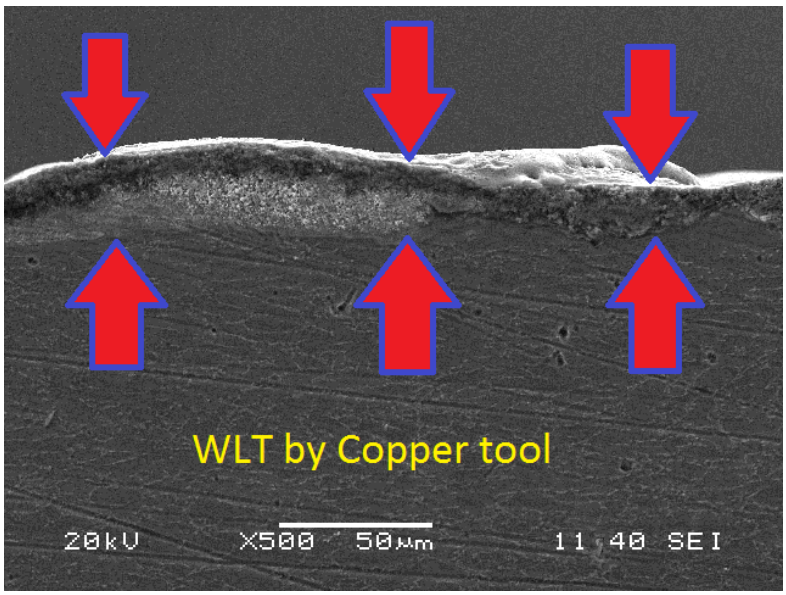

(b) WLT= 20.2074 µm

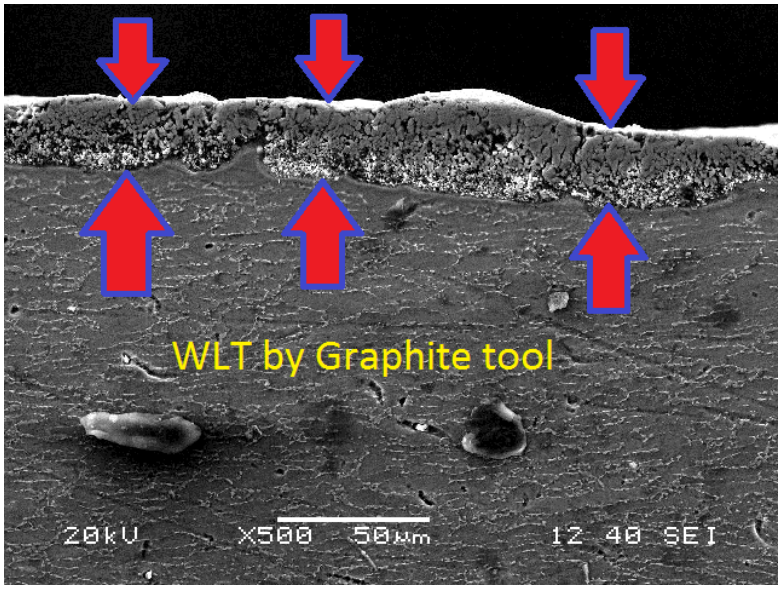

(c) WLT= 21.7504 µm

Fig. 6. WLT on the machined work surface by three electrodes at parameters setting V=20V, I_p=10A, τ=67%, T_{on}=100µs (a) AlSi10Mg SLS, (b) Copper, (c) Graphite

After EDM, metal carbides and oxides like TiC, VC, TiO_2 etc. were observed to form on the machined surfaces and the WLT. These increase the micro-hardness of the WLT. The carbon comes from the separation of hydrocarbon type dielectric fluid EDM-30 oil at the time of sparking process and combines with the debris to form metal carbides on the machined surface. Similarly, oxygen comes from the dielectric fluid present in soluble form or from the environment and forms the metal oxides on the machined surfaces. An increase in the percentage of carbon and oxygen was observed on the machined work surfaces by the energy dispersive X-ray spectroscopy (EDX) analysis shown in Fig. 7. The carbon present on the machined work surface was highest while using the graphite electrode due to the availability of free carbon which dissociates from the electrode and transfers to the freshly generated machined work surface. This explains the high micro-hardness of the WLT on the machined

work surface while using a graphite electrode which follows copper and AlSi10Mg SLS electrodes. Similarly, the electrode elements of Al, Si and Mg were found on the machined work surface while using an AlSi10Mg SLS electrode (see Fig. 7(a)) and the electrode element of Cu was found on the machined work surface while using a copper electrode (see Fig. 7(b)). These electrode elements get transferred onto the machined work surface at the time of spark and electrochemically combine with the removed debris and get deposited as WLT. Overall, the AlSi10Mg SLS electrode performed better in comparison to the two other electrodes as far as the surface integrity and surface topography are considered.

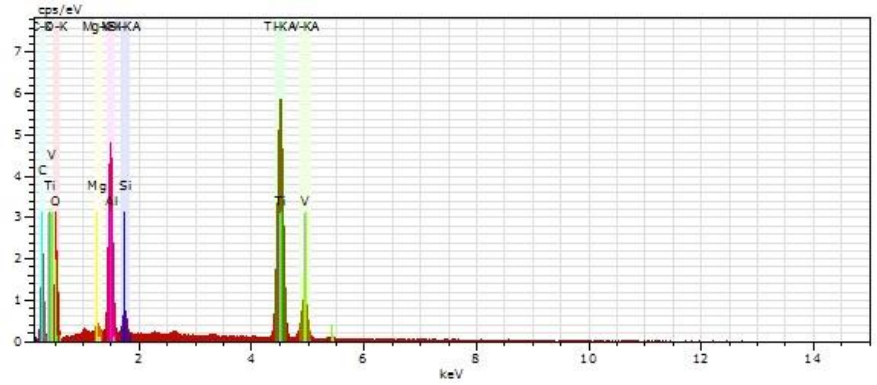

El	norm. C [wt.%]
O	24.67
C	17.21
Ti	44.53
Al	9.46
V	2.40
Si	1.30
Mg	0.44
Total	100.00

(a) AlSi10Mg SLS

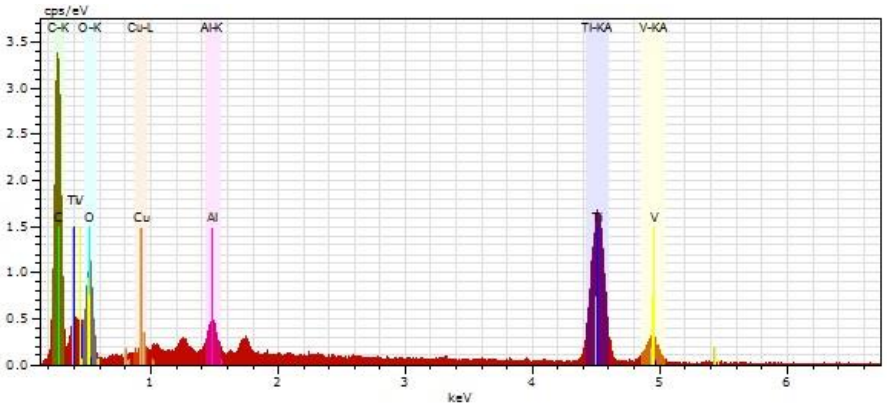

El	norm. C [wt.%]
C	24.25
Ti	54.68
O	15.43
V	2.90
Al	1.48
Cu	1.27
Total	100.00

(b) Copper

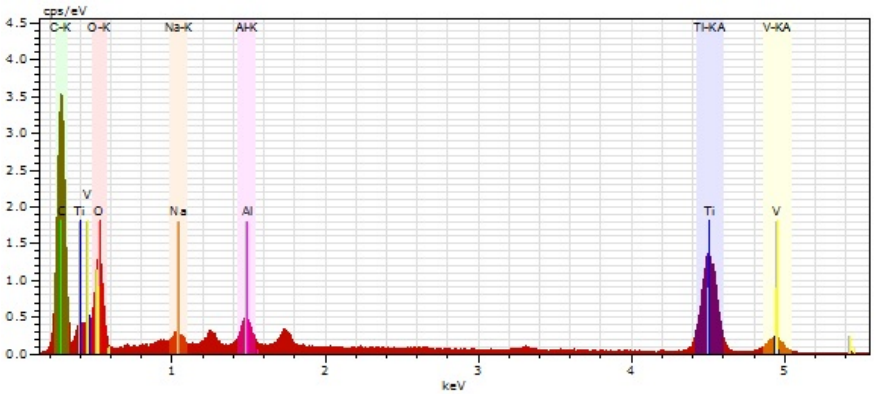

El	norm. C [wt.%]
C	28.03
O	20.19
Ti	46.71
Al	1.93
Na	1.30
V	1.84
Total	100.00

(c) Graphite

Fig. 7. EDX of the machined work surface by three electrodes at parameters setting V=20V, I_p=10A, τ=67%, T_{on}=100µs

5. Conclusions

This experimental investigation introduces a novel hybrid optimisation technique i.e. grey-TOPSIS combined with QPSO applied for the first time to select the best machining parameters and the tool electrode material to machine Ti6Al4V which is by far the most important alloy used in a wide range of aerospace and biomedical applications. The work compared an AlSi10Mg tool electrode newly fabricated by the selective laser sintering method against the traditional copper and graphite electrodes. Multiple performance measures were simultaneously optimized, for instance, material removal rate (MRR) was maximized while the electrode tool wear rate (TWR), average surface roughness (R_a), surface crack density (SCD), white layer thickness (WLT) and micro-hardness (MH) of the machined surface were minimized. The following broad conclusions were obtained:

1. The proposed methodology was found to be a very effective and satisfactory approach for achieving optimal parametric settings for the convoluted electro-discharge machining process. The proposed method proved to be a useful multi-response optimization technique for a wide range of manufacturing industries.
2. From the scanning electron microscope and energy dispersive spectroscopy, it was discovered that among the three tool electrodes material studied, the use of graphite electrode material makes the finished machined surface harder by dissociation of the carbon and subsequent formation of higher order metallic carbides. In terms of machined surface hardness, this was followed by the use of a copper electrode and AlSi10Mg tool electrodes respectively.
3. ANOVA was performed for all the performance measures and closeness coefficient (C_i). Electric current was found to be the most significant parameter affecting the MRR and the MH. The tool electrode material was found to be most influential in affecting the TWR, R_a and SCD. Similarly, pulse-on-time was most influential in affecting the WLT and C_i.
4. The optimal combination of the parametric setting was found to be voltage of 20V, current of 10A, duty cycle of 67%, pulse-on-time of 100 μs and tool electrode materials of AlSi10Mg. These parametric settings allowed for achieving the best combination of MRR,TWR, R_a, SCD, WLT and MH while machining Ti6Al4V using the non-conventional EDM process.

Acknowledgements

AKS and SSM gratefully acknowledge the support provided by CTTC, Bhubaneswar, India for conducting the experimental part. ML is thankful to the support provided by FCT, through IDMEC, under LAETA, project UIDB/50022/2020. SG is particularly thankful to the Research support provided by the UKRI via Grants No. EP/T001100/1 and EP/T024607/1.

References

[1] Shabgard M, Khosrozadeh B. Investigation of carbon nanotube added dielectric on the surface characteristics and machining performance of Ti–6Al–4V alloy in EDM process. *Journal of Manufacturing Processes* 2017; 25:212–219. http://dx.doi.org/10.1016/j.jmapro.2016.11.016

[2] Dewangan S, Gangopadhyay S, Biswas CK. Multi-response optimization of surface integrity characteristics of EDM process using grey-fuzzy logic-based hybrid approach. *Engineering Science and Technology, an International Journal* 2015; 18:361-368. http://dx.doi.org/10.1016/j.jestch.2015.01.009

[3] Uhlmann E, Bergmann A, Bolz R, Gridin W. Application of additive manufactured tungsten carbide tool electrodes in EDM. *Procedia CIRP* 2018; 68:86-90. doi: 10.1016/j.procir.2017.12.027

[4] Stucker BE, Bradley WL, Norasetthekul S, Eubank PT. The production of electrical discharge machining electrodes using SLS: preliminary results, *International Solid Freeform Fabrication Symposium* 1995.

[5] Czelusniak T, Amorim FL, Higa CF, Lohrengel A. Development and application of new composite materials as EDM electrodes manufactured via selective laser sintering. *The International Journal of Advanced Manufacturing Technology* 2014; 72:1503–1512. DOI 10.1007/s00170-014-5765-z

[6] Liu C, Goel S. et al. Benchmarking of several material constitutive models for tribology, wear, and other mechanical deformation simulations of Ti6Al4V. *Journal of the Mechanical Behavior of Biomedical Materials* 2019; 97:126-137. https://doi.org/10.1016/j.jmbbm.2019.05.013

[7] Stolf P, Paiva JM. et al. The role of high-pressure coolant in the wear characteristics of WC-Co tools during the cutting of Ti–6Al–4V. *Wear* 2019; 440–441:203090. https://doi.org/10.1016/j.wear.2019.203090

[8] Bhaumik M, Maity K. Effect of different tool materials during EDM performance of titanium grade 6 alloy. *Engineering Science and Technology, an International Journal* 2018; 21:507-516. https://doi.org/10.1016/j.jestch.2018.04.018

[9] Opoz TT, Yasar H, Ekmekci N, Ekmekci B. Particle migration and surface modification on Ti6Al4V in SiC powder mixed electrical discharge machining. *Journal of Manufacturing Processes* 2018; 31:744–758. https://doi.org/10.1016/j.jmapro.2018.01.002

[10] Kumar S, Batish A, Singh R, Singh TP. A mathematical model to predict material removal rate during electric discharge machining of cryogenically treated titanium alloys. *Proceedings of the Institution of Mechanical Engineers Part B: Journal of Engineering Manufacture* 2015;229(2):214-228. DOI:0.1177/0954405414527955

[11] Sivam SP, Michaelraj AL, Satish KS, Varahamoorthy R, Dinakaran D. Effects of electrical parameters, its interaction and tool geometry in electric discharge machining of titanium grade 5 alloy with graphite tool. *Proceedings of the Institution of Mechanical Engineers Part B: J Engineering Manufacture* 2012; 227(1):119-131. DOI:10.1177/0954405412466213

[12] Sivam SP, Michaelraj AL, Satish KS, Prabhakaran G, Dinakaran D, Ilankumaran V. Statistical multi-objective optimization of electrical discharge machining parameters in machining titanium grade 5 alloy using graphite electrode. *Proceedings of the Institution of Mechanical Engineers Part B: Journal of Engineering Manufacture* 2014; 228(7):736-743. DOI: 10.1177/0954405413511073

[13] Gohil V, Puri YM. Statistical analysis of material removal rate and surface roughness in electrical discharge turning of titanium alloy (Ti-6Al-4V). *Proceedings of the Institution of Mechanical Engineers Part B: Journal of Engineering Manufacture* 2018; 232(9):1603-1614. DOI: 10.1177/0954405416673104

[14] Kolli M, Kumar A. Surfactant and graphite powder–assisted electrical discharge machining of titanium alloy. *Proceedings of the Institution of Mechanical Engineers Part B: Journal of Engineering Manufacture* 2017; 231(4):641-657. DOI: 10.1177/0954405415579019

[15] Sahu AK, Mahapatra SS. Optimization of Electrical Discharge Machining of Titanium Alloy (Ti6Al4V) by Grey Relational Analysis Based Firefly Algorithm. in *Additive Manufacturing of Emerging Materials* (Eds: AlMangour B.). Springer, Cham. 2019, page. 29-53.

[16] Czelusniak T, Amorim FL, Lohrengel A, Higa CF. Development and application of copper–nickel zirconium diboride as EDM electrodes manufactured by selective laser sintering. *The International Journal of Advanced Manufacturing Technology* 2014; 72:905–917. DOI 10.1007/s00170-014-5728-4

[17] Amorim FL, Lohrengel A, Schafer G, Czelusniak T. A study on the SLS manufacturing and experimenting of TiB_2-CuNi EDM electrodes. *Rapid Prototyping Journal* 2013; 19(6):418–429. DOI 10.1108/RPJ-03-2012-0019

[18] Amorim FL, Lohrengel A, Neubert V, Higa CF, Czelusniak T. Selective laser sintering of Mo-CuNi composite to be used as EDM electrode. *Rapid Prototyping Journal* 2014; 20(1): 59–68. DOI 10.1108/RPJ-04-2012-0035

[19] Amorim FL, Lohrengel A, Müller N, Schäfer G, Czelusniak T. Performance of sinking EDM electrodes made by selective laser sintering technique. *The International Journal of Advanced Manufacturing Technology* 2013; 65:1423–1428. DOI 10.1007/s00170-012-4267-0

[20] Durr H, Pilz R, Eleser NS. Rapid tooling of EDM electrodes by means of selective laser sintering. *Computers in Industry* 1999; 39:35–45.

[21] Meena VK, Nagahanumaiah. Optimization of EDM machining parameters using DMLS electrode. *Rapid Prototyping Journal* 2006; 12(4):222–228. DOI 10.1108/13552540610682732

[22] Zhao J, Li Y, Zhang J, Yu C, Zhang Y. Analysis of the wear characteristics of an EDM electrode made by selective laser sintering. *Journal of Materials Processing Technology* 2003; 138:475–478. doi:10.1016/S0924-0136(03)00122-5

[23] Tang Y, Fuh JYH, Lu L, Wong YS, Loh HT, Gupta M. Formation of electrical discharge machining electrode via laser cladding. *Rapid Prototyping Journal* 2002; 8(5):315–319. DOI 10.1108/13552540210451787

[24] Tay FEH, Haider EA. The Potential of Plating Techniques in the Development of Rapid EDM Tooling. *The International Journal of Advanced Manufacturing Technology* 2001; 18:892–896.

[25] Rashid WB, Goel S, Davim JP, Joshi SN. Parametric design optimization of hard turning of AISI 4340 steel (69 HRC). *The International Journal of Advanced Manufacturing Technology* 2016; 82:451–462. DOI 10.1007/s00170-015-7337-2

[26] Deng JL. Introduction to Grey System Theory, The Journal of Grey System 1989; 1:1-24.

[27] Datta S, Mahapatra SS. Modeling, simulation and parametric optimization of wire EDM process using response surface methodology coupled with grey-Taguchi technique. International Journal of Engineering, Science and Technology 2010; 2(5):162-183.

[28] Mohanty CP, Satpathy MP, Mahapatra SS, Singh MR. Optimization of cryo-treated EDM variables using TOPSIS-based TLBO algorithm. *Sadhana* 2018; 43(51):1-18. https://doi.org/10.1007/s12046-018-0829-7

[29] Jadidi O, Hong TS, Firouzi F, Yusuff RM. An optimal grey based approach based on TOPSIS concepts for supplier selection problem. *International Journal of Management Science and Engineering Management* 2009; 4(2):104-117.

[30] Nyaoga R, Magutu P, Wang M. Application of Grey-TOPSIS approach to evaluate value chain performance of tea processing chains. *Decision Science Letters* 2016; 5:431–446.

[31] Sadeghi M, Razavi SH, Saberi N. Application of Grey TOPSIS in preference ordering of action plans in balanced scorecard and strategy map. *Informatica* 2013; 24(4):619–635.

[32] Kennedy J, Eberhart R. Particle swarm optimization. Proceedings of ICNN'95 - *International Conference on Neural Networks*, Perth, WA, Australia, 1995; 4:1942-1948. doi: 10.1109/ICNN.1995.488968.

[33] Mohanty CP, Mahapatra SS, Singh MR. A particle swarm approach for multi-objective optimization of electrical discharge machining process. *Journal of Intelligent Manufacturing*. 2016; 27:1171–1190. DOI 10.1007/s10845-014-0942-3

[34] Sun J, Feng B, Xu W. Particle swarm optimization with particles having quantum behavior. *Proceedings of the 2004 Congress on Evolutionary Computation (IEEE Cat. No.04TH8753)*, Portland, OR, USA, 2004; 1:325-331. doi: 10.1109/CEC.2004.1330875.

[35] Nayak BB, Mahapatra SS. A Quantum Behaved Particle Swarm Approach for Multi-response Optimization of WEDM Process. In: Panigrahi B, Suganthan P, Das S. (eds) *Swarm, Evolutionary, and Memetic Computing. SEMCCO 2014*. Lecture Notes in Computer Science, Springer, Cham. 2015; 8947:62-73. https://doi.org/10.1007/978-3-319-20294-5_6

[36] Mohanty CP, Mahapatra SS, Singh MR. An intelligent approach to optimize the EDM process parameters using utility concept and QPSO algorithm. *Engineering Science and Technology, an International Journal* 2017; 20:552–562. http://dx.doi.org/10.1016/j.jestch.2016.07.003

[37] Omkar SN, Khandelwal R, Ananth TVS, Naik GN, Gopalakrishnan S. Quantum behaved Particle Swarm Optimization (QPSO) for multi-objective design optimization of composite structures. *Expert Systems with Applications* 2009; 36:11312-11322. doi:10.1016/j.eswa.2009.03.006